CRYSTAL GROWTH & DESIGN

pubs.acs.org/crystal

Article

Green Synthesis Approaches toward Preparation of ZIF-76 and Its Thermal Behavior

Published as part of a Crystal Growth and Design virtual special issue on Zeolite Crystal Engineering

Marija Švegovec, Aljaž Škrjanc, Andraž Krajnc, and Nataša Zabukovec Logar*

Cite This: *Cryst. Growth Des.* 2023, 23, 3754−3760

Read Online

ACCESS | Metrics & More | Article Recommendations | Supporting Information

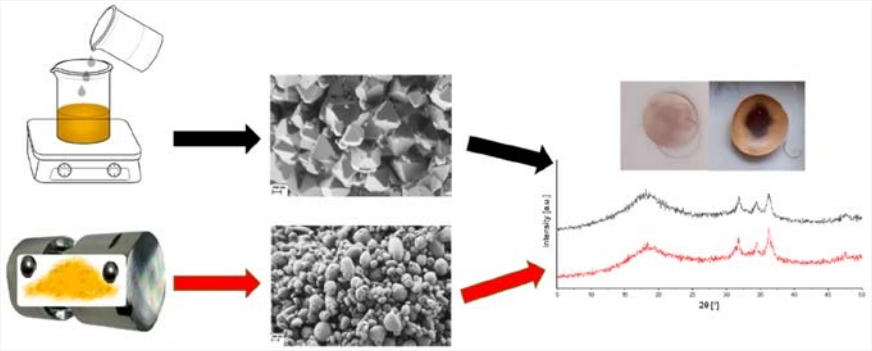

ABSTRACT: With the current increase of interest in amorphous MOFs and ZIFs for various applications, there is a need for optimal and environmentally friendly synthesis of the parent materials. One of the ZIFs that has received the most research to date, along with ZIF-62, is ZIF-76. ZIF-62 has already been produced mechanochemically, while the majority of ZIF-76 is currently produced using solvothermal synthesis in an autoclave with DMF as the solvent. Herein, we present two new green synthesis methods for creating a ZIF-76 framework. The mechanochemical and precipitation approaches were developed to shorten reaction times and allow for room temperature synthesis. This work represents the first step toward green synthesis of ZIF-76 and its thermally treated variants.

INTRODUCTION

Metal−organic frameworks (MOFs) are a class of highly porous materials that are truly unique in their degree of structural diversity, tunability, and variety of chemical and physical properties. These materials are renowned for their chemical versatility and are composed of metal nodes connected by organic ligands in infinite arrays.[1,2] They are widely used for gas sorption and separation, catalysis, and drug delivery.[3−8]

The family of MOFs known as zeolitic imidazolate frameworks (ZIFs) is of tremendous interest due to its chemical stability and structural similarities to zeolites. When compared to their inorganic counterparts, like zeolites, ZIFs exhibit different mechanical properties[9] and can structurally collapse upon heating, pressurization, or ball milling.[10] However, some zinc- and cobalt-based zeolitic imidazolate frameworks have high thermal stability; they melt before thermal decomposition and form amorphous frameworks that have the same short-range connectivity as their crystalline counterparts.[2,11−13] ZIF glasses, a new family of inorganic−organic glasses, are produced by rapidly cooling a ZIF liquid from above its melting temperature (T_m) to below its glass transition temperature (T_g).[1]

The glass forming ability (GFA), which is determined by the T_g/T_m ratio and is typically inversely related to the liquid fragility m, is the ability of a liquid to avoid crystallization during cooling.[14] Based on the Kauzmann "2/3 Law", systems with $T_g/T_m > 2/3$ surpass the practical limits of the supercooled state and are thus likely to find their way to the future applications.[15]

ZIFs are known to have an extremely high GFA, exceeding values of 0.8.[16] For example, commonly used SiO_2, PMMA, and B_2O_3 show a GFA of around 0.75.[16]

ZIF-76 is a mixed-linker ZIF composed of zinc coordinated by a mixture of imidazole (Im) and 5-chlorobenzimidazole (5-ClbIm) as ligands to form a three-dimensional framework with LTA topology.[17] It comprises a pore aperture and pore diameter of 5.4 and 12.2 Å, respectively.[18] Although most MOFs do not melt when heated, it has been found that under certain

Received: February 10, 2023
Revised: April 6, 2023
Published: April 20, 2023

https://doi.org/10.1021/acs.cgd.3c00137
Cryst. Growth Des. 2023, 23, 3754−3760

conditions ZIF-76 can melt and be quenched to an a_gZIF-76 (a_g signifies amorphous glass).[19,20]

The current synthetic procedures for the synthesis of ZIF-76 are solvothermal, frequently requiring large quantities of N,N-dimethylformamide (DMF) or diethyl formamide (DEF),[19,21] which are proven teratogens with negative impacts on human health and environmental risks due to their inherent toxicity, as well as needing enormous wastewater streams and a significant energy input.[22] Eliminating organic solvents or substituting less harmful solvents for these hazardous ones is one of the most significant green chemistry concerns.[23] Additionally, solvothermal synthesis of ZIFs takes between 48 and 96 h, requires high synthesis temperatures, and typically results in low yields.[16]

Mechanochemistry is a strong contender as a replacement for traditional solution-based chemistry. Recent advances in mechanochemistry have made it possible to synthesize materials at room temperature without the need of large quantities of solvents and with excellent yields while also being ecologically benign.[24,25]

Therefore, the objective of this work was to successfully synthesize ZIF-76 using a mechanochemical method and a green solvothermal synthesis that replaces DMF with gamma-valerolactone (GVL). GVL, which can be easily generated from lignocellulosic biomass, is regarded as a green solvent due to its renewability, biodegradability, and nontoxicity.[22] It has low melting (−31 °C), high boiling (207 °C) and flash (96 °C) points, and because GVL does not react with water at temperatures above 60 °C for several weeks, it can be utilized as a green solvent under mild conditions.[26]

EXPERIMENTAL SECTION

Materials. Imidazole (99%), $Zn(OAc)_2{\cdot}2H_2O$ (98%), and ZnO (<100 nm) were purchased from Aldrich. $Zn(NO_3)_2{\cdot}6H_2O$ (98%), gamma-valerolactone (99%), and sodium hydroxide were purchased from Sigma-Aldrich. 5-Chlorobenzimidazole (97%) was purchased from Fluorochem. Ethanol was purchased from Stella TECH. Methanol was purchased from Honeywell Riedel-de Haen. All materials were used without further purification. Water was deionized in-house.

Green Precipitation Synthesis. ZIF-76 was synthesized by modification of the solvothermal DMF synthesis.[18] The synthesis mixture was prepared by mixing together 16.5 mL of GVL/MeOH, 0.24 g of Im, 0.25 g of 5-ClbIm (Im/5-ClbIm molar ratio of 3:1), and 0.5 g of $Zn(NO_3)_2{\cdot}6H_2O$ in a glass bottle for 1 h. Following the addition of NaOH(aq) (1 mL, 2.5 M), the reaction mixture was stirred at room temperature overnight. After filtering the mixture, ethanol was used to wash the sample. To activate ZIF-76, the material was soaked in methanol for 24 h to exchange the GVL for methanol. To remove the solvent trapped in the pores, the samples were put in a vacuum oven under a static vacuum at 140 °C overnight. The so prepared optimized samples used for further analyses were named ZIF-76 RT. Additional synthesis information can be found in the Supporting Information.

Mechanochemical Synthesis. All of the reagents needed for the synthesis with the ratio of linkers being 1:1 were added to a 10 mL stainless steel grinding jar, together with two 10 mm stainless steel grinding balls (Table S-1). The grinding jar was sealed and shaken at 30 Hz for 40 min on a Retsch MM400 mixer mill. After grinding, the jars were opened and the powder extracted. Centrifugation was used to isolate the products, which were then washed with ethanol and dried overnight at 60 °C. The so prepared optimized samples used for further analyses were named ZIF-76 BM. Additional synthesis information can be found in the Supporting Information.

Thermal Sintering Procedure. About 15 mg of the ZIF-76 RT and ZIF-76 BM samples was pressed into pellets using a stainless-steel mold (0.8 cm in diameter) pressed in a hydraulic press for 1 min with a pressure of 3 tonnes. Pelletized samples were placed in a ceramic crucible and then into an argon-purged muffle furnace before being heated at 10 °C min^{-1} to 400 °C. Once the temperature was reached, the furnace was turned off, and the samples were allowed to cool naturally (under argon) to room temperature. The so prepared optimized samples used for further analyses were named ZIF-76 RT 400 and ZIF-76 BM 400, respectively.

Materials Characterization. *Powder X-ray Diffraction (PXRD).* Powder X-ray diffraction data were acquired with a PANanalytical X'Pert PRO high-resolution diffractometer using Cu Kα1 radiation (1.5406 Å) in the 2θ range from 5 to 50° (100 s per step of 0.033°) with a fully open X'Celerator detector. The diffractograms were analyzed by X'Pert HighScore Plus 4.9 Program.

Scanning Electron Microscopy (SEM). Morphology and size of the crystals were determined by scanning electron microscopy using a Zeiss Supra 35 VP microscope with an electron high tension voltage of 1.00 kV and an aperture size of 30.00 μm.

Liquid Nuclear Magnetic Resonance (NMR). Proton NMR was recorded using an AVANCE NEO Bruker 400 MHz spectrometer at room temperature. Approximately 1.5 mg of each sample was digested in a mixture of DCl (35%)/D_2O (0.1 mL) and DMSO (0.5 mL). Data analysis was performed using the MestreNova software package.

Thermogravimetric Analysis (TG) and Differential Scanning Calorimetry (DSC). Thermogravimetric analysis was performed using a TA Instruments Q5000. Measurements were performed in a continuous air stream (25 mL/min air, 10 mL/min Ar), with samples heated from 25 to 700 °C at a rate of 10 °C/min. DSC analysis of all samples was performed using a TA Instruments Q2000 MDSC. The samples were placed in an aluminum crucible on a DSC sample holder at room temperature. The samples were heated at 10 °C/min to 450 °C. After cooling to room temperature at 10 °C/min, the second upscan was performed using the same procedure as the first. Data analysis was performed using TA Instruments' TRIOS software.

Nitrogen Physisorption (BET). Using the Autosorb iQ3, nitrogen physisorption isotherms were recorded at −196 °C. The samples were degassed for 10 h at 130 °C under a vacuum prior to the adsorption analysis. From adsorption data in the relative pressure range of 0.05 to 0.2, the Brunauer−Emmett−Teller (BET) specific surface area was calculated. The amount of N_2 adsorbed at P/P_0 = 0.97 was used to determine the total pore volume (V_{total}) while the micropore volume was calculated using the t-plot in the p/p_0 range from 0.15 to 0.3. The software's built-in functions were used for all mentioned calculations.

Dynamic Vapor Sorption (DVS) Analysis. CO_2 and H_2O isotherms were collected on a Surface Measurements Systems DVS Vacuum. The samples were first degassed at 110 °C in a vacuum with the turbo pump on for 10 h then left to cool under a vacuum for 3 h. The isotherms were collected at 30 °C in the pressure ranges P/P_0 from 0 to 90 for water and 0 to 100 for CO_2. P_{0H_2O} was 31.5 Torr, and P_{0CO_2} was 760 Torr. Humid CO_2 isotherms were collected by adding a first step where water vapor was added to the pressure, where at the final point the desired humidity would be achieved. The CO_2 isotherms were then collected the same way as for dry CO_2.

RESULTS AND DISCUSSION

Synthesis of Phase Pure Materials. Based on our past success with gamma-valerolactone (GVL) as a DMF alternative,[27] we attempted a traditional solvothermal synthesis with DMF substituted by a 1:1 GVL/MeOH mixture. No product was formed in the reaction. We speculated that this was due to a deficiency of the base formed during the thermal decomposition of DMF. This hypothesis was tested by adding an aqueous solution of NaOH, which was previously used to adjust the pH of the reaction mixture to a basic level, which promotes the condensation of imidazole-based ligands and metal ions to form ZIF crystals. The amount and concentration of NaOH used can impact the size, shape, and crystallinity of the resulting ZIFs. Too much NaOH can cause overcondensation and ZIF aggregation, while too little NaOH can cause an insufficient reaction and low yield.[28−30] We chose to use 1 mL of NaOH

https://doi.org/10.1021/acs.cgd.3c00137
Cryst. Growth Des. 2023, 23, 3754−3760

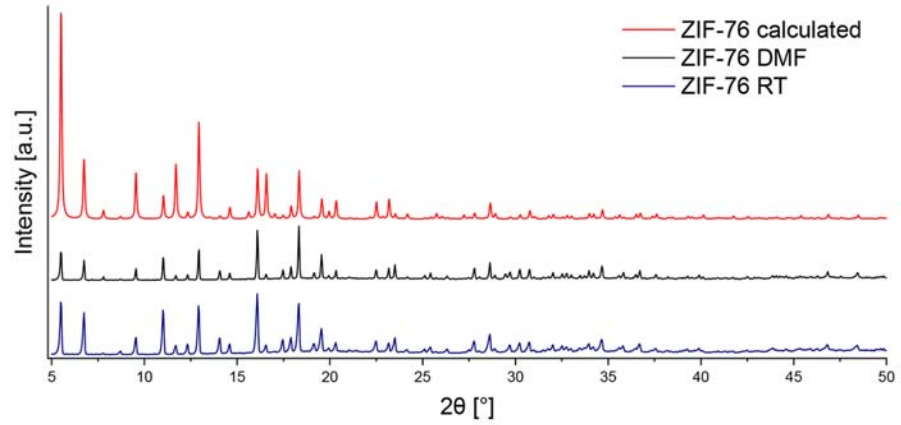

Figure 1. PXRD of calculated (red), DMF-synthesized (black), and GVL-synthesized (blue) ZIF-76.

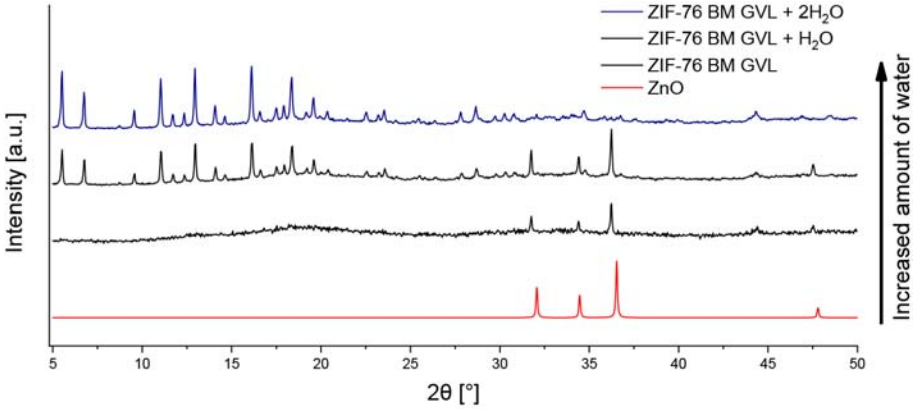

Figure 2. PXRD of ball-milled ZIF-76 BM with increasing water addition.

solution as it represents 0.5 equiv to the combined molar amount of linkers in the solution. The syntheses were also carried out with 1 equiv and 0.25 equiv of NaOH. The results revealed that using 1 equiv did not significantly differ from using 0.5 equiv, as the obtained yield for both reactions was only 47%, indicating that doubling the amount of base added was not required. However, when 0.25 equiv of NaOH was used, precipitation began after 1 h of stirring, whereas with 0.5 equiv, precipitation began almost immediately after the addition of a base. A significant decrease in yield, down to 33%, was observed upon reducing the amount of base. Additionally, PXRD analysis of the samples indicated slightly wider peaks for the 0.25 equiv in comparison to the 0.5 equiv. PXRD analysis of the product showed that ZIF-76 RT was finally obtained.

When the diffraction patterns of the differently synthesized ZIF-76 samples are compared (Figure 1), it can be observed that the green-synthesis samples display a significant level of crystallinity, as evidenced by the comparison of full width at half maximum (fwhm) of the initial peaks. The major peak intensities appear to have shifted in comparison to the simulated sample. This is likely due to variations in the linker ratio of the structures available in the CCDC database. All of the diffraction patterns are in good agreement with the calculated diffraction pattern, and at low angles no additional peaks were observed that could indicate the formation of another crystalline ZIF phase, providing solid proof of the successful synthesis of the ZIF-76 RT. Sodium formate, sodium carbonate, and ammonia were also tested as bases with either no precipitation occurring or significantly decreased yields in the final products.

Since GVL was used effectively in the solvothermal synthesis, we opted to use it as the primary solvent in liquid assisted grinding (LAG). PXRD analysis of the sample after using only 100 μL of GVL as the solvent showed that primarily ZnO was formed, along with some unidentified amorphous phase (Figure 2).

The addition of 50 μL of water resulted in increased crystallinity and the partial synthesis of ZIF-76 BM from ZnO. We hypothesize that water helps in the ligand deprotonation step. The addition of a double of the initial amount of the water resulted in the complete conversion of ZnO to the desired framework, with a yield of 94%, which is significantly higher than the yield obtained through room temperature synthesis (Figure 2). Furthermore, NaOH was used during mechanochemical synthesis, but there was no significant improvement in yield or crystallinity. The Scherrer equation was used to conduct a quantitative analysis to determine crystallite size, with the calculated size for the DMF, RT, and BM samples being 600, 300, and 80 nm, respectively.

In order to determine how various synthesis methods, affect the size and shape of the crystals, scanning electron microscopy was used and the size and morphology of the ZIF-76 samples was examined (Figure 3). Both products appear to be in the pure phase, with some traces of unreacted components or impurities present in the BM sample. The ball-milled ZIF-76 BM particles exhibit a smaller ellipsoidal particle morphology, and the SEM

https://doi.org/10.1021/acs.cgd.3c00137
Cryst. Growth Des. 2023, 23, 3754−3760

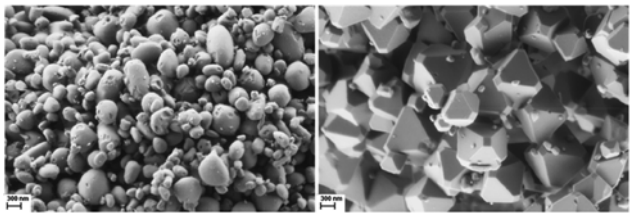

Figure 3. SEM images of the ball-milled (BM; left) and the precipitated (RT; right) ZIF-76.

images of the particles revealed their irregular size distribution. The formation of polycrystalline ellipsoidal particles in materials prepared by BM may be explained by the densely packed structures that arise due to the repeated stress caused by the rotating balls in the milling jars.[31] The precipitated ZIF-76 RT particles showed a truncated octahedron shape and somewhat smooth surfaces indicating that the particles were well crystallized.

After comparing the calculated particle size from XRD to the SEM-determined particle size for BM product, we can infer that the individual ellipsoidal particles are created from multiple crystallite particles that have agglomerated together. On the other hand, the agreement between the calculated and SEM-determined particle sizes of the RT products suggests that the particles are composed of a single crystallite.

The permanent porosity was investigated by using N_2 physisorption. The adsorption isotherms and pore size distribution for both ZIF-76 samples are shown in Figure 4. The software's built-in functions were used to calculate the BET surface area, total pore volume, and micropore volume (Table 1).

Both samples exhibit a type I isotherm, typical for microporous materials. BET surface areas of 827 $m^2\ g^{-1}$ and 526 $m^2\ g^{-1}$, respectively for precipitated ZIF-76 RT and the ball-milled sample, were calculated from N_2 adsorption isotherms at 77 K. We performed liquid NMR analysis to confirm the ligand ratio in the samples because the S_{BET} values were lower than anticipated.[30]

Acid-digested ^{1}H NMR spectroscopy offers helpful information regarding the integrity of the linkers as well as the linker stoichiometry in the framework for ZIFs or MOFs with mixed linkers, such as ZIF-76. The ^{1}H NMR spectra for the precipitated ZIF-76 RT and ZIF-76 BM samples revealed a similar structure in both samples (Figure S-7).

The protons of the imidazole are attributed to the peak at 8.9 ppm, and the protons of the benzimidazole appear at roughly 9.5 ppm. These peaks are at similar positions to those in earlier NMR spectra that have been reported.[30] The isolated proton peaks in imidazole and 5-chlorobenzimidazole are helpful for determining the ligand ratio. The ratio was calculated by comparing the integrals of the peaks labeled "H_a" and "H_b" in Figure S-7. For each material, the ratio of imidazole to the 5-chlorobenzimidazole ligand was 1, which was expected for the ball-milled sample due to the initial ligand ratio being 1:1. However, it is less than the value of 3 for the Im/5-ClbIm ratio that was previously reported for the solvothermal synthesis.[18] We attempted to evaluate this phenomenon in the precipitation method by using a different ratio (7:1) of ligands in the synthesis mixture (Table S-2). The additional ^{1}H NMR spectra (Figure S-8) show that the obtained ligand ratio is 1:1.7, again lower than expected from the synthesis ratio, which could be explained by linker acidity. Because the 5-ClbIm linker has a lower pK_a value

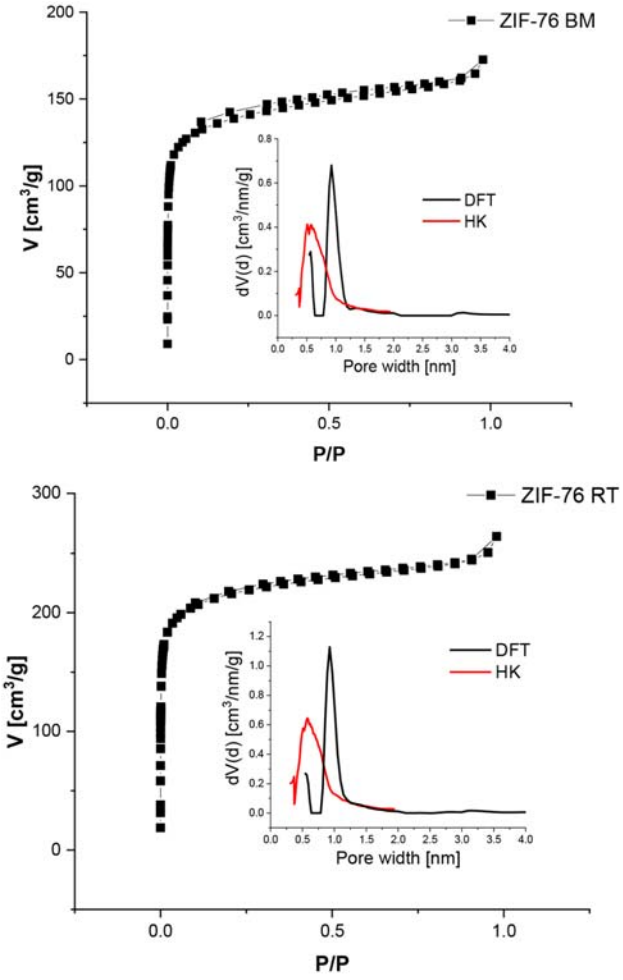

Figure 4. N_2 adsorption isotherms for precipitated (up) and ball-milled (down) ZIF-76. The inset shows pore size distribution graphs calculated from nitrogen physisorption isotherms.

Table 1. Calculated Brunauer–Emmett–Teller (BET) Surface Area, Total Pore Volume, and Micropore Volume

ZIF	S_{BET} ($m^2\ g^{-1}$)[a]	V_{total} ($cm^3\ g^{-1}$)[b]	V_{micro} ($cm^3\ g^{-1}$)[c]
ZIF-76 RT	827	0.409	0.266
ZIF-76 BM	526	0.268	0.166

[a]S_{BET}: Specific surface area was calculated by the BET method using adsorption data in the range of P/P_0 = 0.05–0.2. [b]V_{total}: Total pore volume was calculated based on the nitrogen adsorption amount at p/p_0 = 0.97. [c]Micropore volume.

than the imidazole linker,[32,33] it is more acidic and thus more susceptible to deprotonation. This deprotonation makes it easier for the linker to form a stable 1:1 product because the deprotonated species can interact with other species in the system more effectively, resulting in a more stable framework.

Thermal Properties. Both materials are stable up to 400 °C in an inert atmosphere, as determined by the thermal analysis reported in Figure S-1. According to an accompanying differential scanning calorimetry (DSC) analysis, the precipitated sample showed an endothermic peak attributed to melting with an onset temperature of 360 °C and an endset temperature of 431 °C, while the ball-milled sample showed a peak for melting with an onset temperature of 362 °C and an endset temperature of 440 °C (Figure 5). These results are consistent

https://doi.org/10.1021/acs.cgd.3c00137
Cryst. Growth Des. 2023, 23, 3754–3760

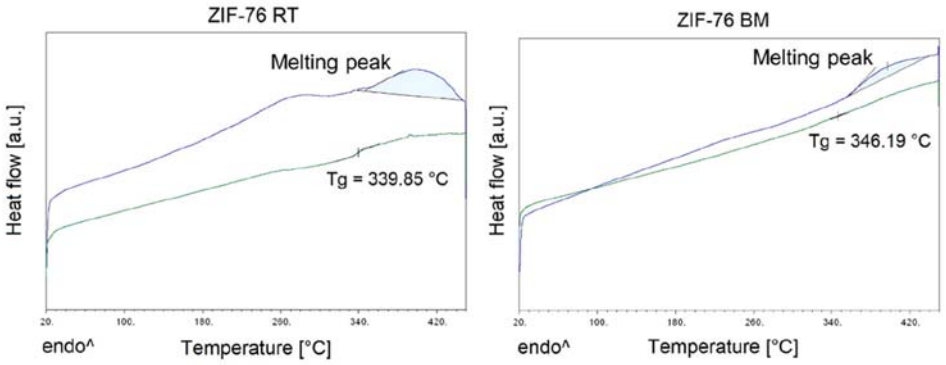

Figure 5. DSC curves showing first upscan (blue) and the second upscan (green) of the precipitated (left) and ball-milled ZIF-76 (right).

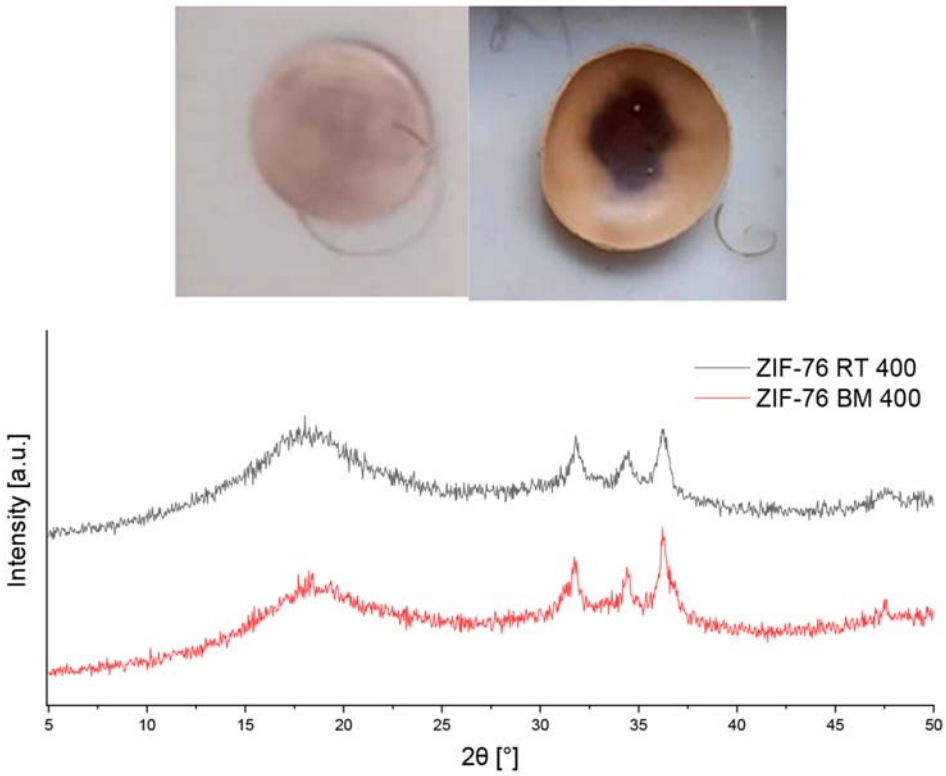

Figure 6. Pellet before and after vitrification (up) and PXRD of precipitated (black) and ball-milled (red) ZIF-76 after vitrification (down).

with previously published data.[19,30] The PXRD pattern of ZIF-76 RT quenched at ambient temperature exhibits a broad peak at $2\theta \approx 18°$, indicating the material's amorphous nature (Figure S-2). The findings show that both ZIF-76 RT and BM can be melt-quenched to form a_gZIF-76. Glass transition peaks for the precipitated sample and the ball-milled sample can be seen on the DSC upscan of the glassy a_gZIF-76 at T_g = 339 and 347 °C, respectively. These reported values for both a_gZIF-76 RT and BM were found to be higher than expected,[19,30] which was attributed to the higher 5-ClbIm linker content in the samples. The precipitated ZIF-76 RT exhibits a small endotherm peak due to the desolvation of the residual solvent (Figure 5).

Preliminary Vitrification Results. Glass formation ability was tested for both samples, ZIF-76 RT and ZIF-76 BM. Due to ZIF-76's lack of a liquid stage in melting,[34] samples were pelletized before thermal treatment in a muffle furnace. The pelletized samples were then heated to 400 °C in argon and left to cool to room temperature. The sample pellets (Figure 6) noticeably darkened and gained a shine, which could indicate that glass formation occurred. PXRD was used to check if amorphization occurred and to check for possible ZnO formation. The broad peak that can be attributed to a_gZIF-76 can be observed for both samples, with both also exhibiting some characterizing ZnO diffraction peaks. The estimation of ZnO in the amorphous phases was carried out by integrating the amorphous background and the signal peaks, which led to an approximate estimation of 1−3% of ZnO in the vitrified samples. The presence of ZnO can be attributed to possible leaks of air into the muffle furnace causing the thermal decomposition of the surface of the pellet. Solution ^{1}H NMR spectroscopy showed that the linker ratio values of the parent crystalline material were preserved in all a_gZIF-76 samples following vitrification. Despite DSC results and literature data implying that vitrification would occur even after multiple attempts with varying temperatures

https://doi.org/10.1021/acs.cgd.3c00137
Cryst. Growth Des. 2023, 23, 3754−3760

and programs, clear glass could not be prepared. SEM imaging of the thermally treated pellets showed clear signs of a sintering-like process occurring on the surface, which was observed even at lower temperatures down to 380 °C. This is most clearly visible in Figure 7 where the filling of the interparticle space and melding of surface particles is observed in SEM imaging.

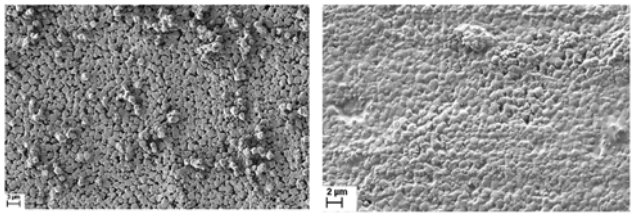

Figure 7. SEM imaging of surfaces of untreated (left) and thermally treated (right) pellets of ZIF-76-RT.

CO_2 and Water Vapor Sorption Evaluation. Due to the limited sample amounts available for our particular adsorber setup, we did not perform nitrogen physisorption on the samples. Instead, we collected CO_2 isotherms, which require less of a sample. CO_2 isotherms were collected at 30 °C for both samples before and after vitrification to confirm the presence/retention of porosity. The uptakes of samples before vitrification were 0.94 and 0.73 mmol/g for crystalline ZIF-76 RT and ZIF-76 BM, respectively (Figure S-9). The uptakes of thermally treated samples (Figure S-11) noticeably dropped to 0.33 mmol/g for ZIF-76 RT and 0.23 mmol/g for ZIF-76 BM. Due to the lack of comparable literature data on CO_2 isotherms at 30 °C, a ZIF-8 sample was analyzed under the same conditions for comparison and revealed the uptake of 0.56 mmol/g.

Water isotherms for both crystalline samples were also collected (Figure S-10), and both showed low water uptake, with the ZIF-76 RT sample showing a slightly higher value. The higher final uptake for ZIF-76 RT can be associated with higher porosity, as determined from N_2 and CO_2 isotherms. On the other hand, the shape of the isotherm implies a more hydrophilic character of the ZIF-76 BM sample (type I isotherm), which could be due to the presence of more defects in the structure.

An increase in mass was observed in the desorption part of the water isotherm, which coincided with a loss of crystallinity after measurement as proved by the XRD analysis (Figure S-3). This could potentially be attributed to water mediated decomposition of the product.

We also collected CO_2 isotherms at 50% RH (Figure S-12). No significant change in CO_2 uptake was observed in the BM sample, while the RT sample had a significant reduction due to higher water adsorption. Both vitrified samples, while showing reduced uptake, still exhibit high enough CO_2 uptakes to indicate the retention of porosity.

CONCLUSION

In this work, we present two novel green synthesis approaches toward preparation of ZIF-76 framework material with permanent porosity. It was shown that the synthesis of ZIF-76 can be done at room temperature utilizing an environmentally friendly solvent and mechanochemically with a high yield if compared to DMF/DEF-based synthesis. ^{1}H NMR of the precipitated ZIF-76 showed an increased 5-ClbIm to Im ratio as compared to regular DMF solvothermal synthesis. This could explain the lower S_{BET} for both ZIF-76 RT and ZIF-76 BM samples if compared to the literature data.[30] DSC analysis of the samples showed that both products have a peak associated with a glass transition temperature, and PXRD of the samples after DSC showed no presence of ZnO, only a broad peak, which is characteristic of amorphous materials. However, initial thermal treatment tests resulted in some ZnO formation likely as a result of leaks in the furnace. While vitrification was not successful, a thermal sintering-like process was detected for both ZIFs, suggesting that this could still be used as an alternative for processing and addressing powder-handling concerns in industrial settings, as well as composite fabrication. The CO_2 and water isotherms collected for the samples before thermal treatment and CO_2 isotherms collected after sintering show that the materials are porous and preferentially hydrophobic. This opens the possibility for the use of a_gZIF-76 as a composite material with different porous materials, thermally stable at 380−400 °C. Making ZIF composites may improve their adsorption ability, as their current instability in high humidity and tendency to adsorb water have limited their use as CO_2 adsorbents.

ASSOCIATED CONTENT

Supporting Information

The Supporting Information is available free of charge at https://pubs.acs.org/doi/10.1021/acs.cgd.3c00137.

Reagents used in mechanochemical synthesis (Table S1); reagents required for the precipitation synthesis (Table S2); PXRD, TG, ^{1}H NMR, and adsorption isotherms (Figures S1−S12) (PDF)

AUTHOR INFORMATION

Corresponding Author

Nataša Zabukovec Logar − *National Institute of Chemistry, SI-1001 Ljubljana, Slovenia; University of Nova Gorica, SI-5000 Nova Gorica, Slovenia;* orcid.org/0000-0001-8972-0087; Email: natasa.zabukovec@ki.si

Authors

Marija Švegovec − *National Institute of Chemistry, SI-1001 Ljubljana, Slovenia; University of Nova Gorica, SI-5000 Nova Gorica, Slovenia*

Aljaž Škrjanc − *National Institute of Chemistry, SI-1001 Ljubljana, Slovenia; University of Nova Gorica, SI-5000 Nova Gorica, Slovenia*

Andraž Krajnc − *National Institute of Chemistry, SI-1001 Ljubljana, Slovenia;* orcid.org/0000-0003-2249-602X

Complete contact information is available at: https://pubs.acs.org/10.1021/acs.cgd.3c00137

Author Contributions

The manuscript was written through contributions of all authors. All authors have given approval to the final version of the manuscript.

Funding

This research was funded by Slovenian Research Agency Research program P1-0021.

Notes

The authors declare no competing financial interest.

■ ACKNOWLEDGMENTS

The authors would like to thank Mojca Opresnik for SEM measurements, Edi Kranjc for XRD measurements, and Uroš Javornik for help with liquid NMR.

■ REFERENCES

(1) Frentzel-Beyme, L.; Kloß, M.; Kolodzeiski, P.; Pallach, R.; Henke, S. Meltable Mixed-Linker Zeolitic Imidazolate Frameworks and Their Microporous Glasses: From Melting Point Engineering to Selective Hydrocarbon Sorption. *J. Am. Chem. Soc.* **2019**, *141* (31), 12362−12371.

(2) Bennett, T. D.; Yue, Y.; Li, P.; Qiao, A.; Tao, H.; Greaves, N. G.; Richards, T.; Lampronti, G. I.; Redfern, S. A. T.; Blanc, F.; Farha, O. K.; Hupp, J. T.; Cheetham, A. K.; Keen, D. A. Melt-Quenched Glasses of Metal-Organic Frameworks. *J. Am. Chem. Soc.* **2016**, *138* (10), 3484−3492.

(3) Li, Y.; Wang, Y.; Fan, W.; Sun, D. Flexible Metal-Organic Frameworks for Gas Storage and Separation. *Dalton Transactions* **2022**, *51*, 4608−4618.

(4) Qian, Q.; Asinger, P. A.; Lee, M. J.; Han, G.; Mizrahi Rodriguez, K.; Lin, S.; Benedetti, F. M.; Wu, A. X.; Chi, W. S.; Smith, Z. P. MOF-Based Membranes for Gas Separations. *Chem. Rev.* **2020**, *120*, 8161−8266.

(5) Konnerth, H.; Matsagar, B. M.; Chen, S. S.; Prechtl, M. H. G.; Shieh, F. K.; Wu, K. C. W. Metal-Organic Framework (MOF)-Derived Catalysts for Fine Chemical Production. *Coord. Chem. Rev.* **2020**, *416*, 213319.

(6) Mallakpour, S.; Nikkhoo, E.; Hussain, C. M. Application of MOF Materials as Drug Delivery Systems for Cancer Therapy and Dermal Treatment. *Coord. Chem. Rev.* **2022**, *451*, 214262.

(7) Yoon, M.; Srirambalaji, R.; Kim, K. Homochiral Metal-Organic Frameworks for Asymmetric Heterogeneous Catalysis. *Chem. Rev.* **2012**, *112*, 1196−1231.

(8) Horcajada, P.; Gref, R.; Baati, T.; Allan, P. K.; Maurin, G.; Couvreur, P.; Férey, G.; Morris, R. E.; Serre, C. Metal-Organic Frameworks in Biomedicine. *Chem. Rev.* **2012**, *112*, 1232−1268.

(9) Schneemann, A.; Bon, V.; Schwedler, I.; Senkovska, I.; Kaskel, S.; Fischer, R. A. Flexible Metal-Organic Frameworks. *Chem. Soc. Rev.* **2014**, *43*, 6062.

(10) James, S. L.; Friščic, T. Mechanochemistry. *Chem. Soc. Rev.* **2013**, *42* (18), 7494−7496.

(11) Frentzel-Beyme, L.; Kloß, M.; Pallach, R.; Salamon, S.; Moldenhauer, H.; Landers, J.; Wende, H.; Debus, J.; Henke, S. Porous Purple Glass-a Cobalt Imidazolate Glass with Accessible Porosity from a Meltable Cobalt Imidazolate Framework. *J. Mater. Chem. A Mater.* **2019**, *7* (3), 985−990.

(12) Tao, H.; Bennett, T. D.; Yue, Y. Melt-Quenched Hybrid Glasses from Metal−Organic Frameworks. *Adv. Mater.* **2017**, *29* (20), 1601705.

(13) Gaillac, R.; Pullumbi, P.; Beyer, K. A.; Chapman, K.; Keen, D. A.; Bennett, T. D.; Coudert, F. X. Liquid Metal−Organic Frameworks. *Nat. Mater.* **2017**, *16* (11), 1149−1155.

(14) Fonseca, J.; Gong, T.; Jiao, L.; Jiang, H. L. Metal-Organic Frameworks (MOFs) beyond Crystallinity: Amorphous MOFs, MOF Liquids and MOF Glasses. *Journal of Materials Chemistry A.* **2021**, *9*, 10562−10611.

(15) Yu, Z.; Tang, L.; Ma, N.; Horike, S.; Chen, W. Recent Progress of Amorphous and Glassy Coordination Polymers. *Coord. Chem. Rev.* **2022**, *469*, 214646.

(16) Qiao, A.; Bennett, T. D.; Tao, H.; Krajnc, A.; Mali, G.; Doherty, C. M.; Thornton, A. W.; Mauro, J. C.; Greaves, G. N.; Yue, Y. A Metal-Organic Framework with Ultrahigh Glass-Forming Ability. *Sci. Adv.* **2018**, *4* (3), DOI: 10.1126/sciadv.aao6827.

(17) Baerlocher, C.; Mccusker, L. B.; Olson, D. H. *Atlas of Zeolite Framework Types*; Elsevier B.V., 2007. DOI: 10.1016/B978-0-444-53064-6.X5186-X.

(18) Banerjee, R.; Phan, A.; Wang, B.; Knobler, C.; Furukawa, H.; O'Keeffe, M.; Yaghi, O. M. High-Throughput Synthesis of Zeolitic Imidazolate Frameworks and Application to CO2 Capture. *Science (1979)* **2008**, *319* (5865), 939−943.

(19) Zhou, C.; Longley, L.; Krajnc, A.; Smales, G. J.; Qiao, A.; Erucar, I.; Doherty, C. M.; Thornton, A. W.; Hill, A. J.; Ashling, C. W.; Qazvini, O. T.; Lee, S. J.; Chater, P. A.; Terrill, N. J.; Smith, A. J.; Yue, Y.; Mali, G.; Keen, D. A.; Telfer, S. G.; Bennett, T. D. Metal-Organic Framework Glasses with Permanent Accessible Porosity. *Nat. Commun.* **2018**, *9* (1), 5042 DOI: 10.1038/s41467-018-07532-z.

(20) Li, S.; Limbach, R.; Longley, L.; Shirzadi, A. A.; Walmsley, J. C.; Johnstone, D. N.; Midgley, P. A.; Wondraczek, L.; Bennett, T. D. Mechanical Properties and Processing Techniques of Bulk Metal-Organic Framework Glasses. *J. Am. Chem. Soc.* **2019**, *141* (2), 1027−1034.

(21) Nozari, V.; Smirnova, O.; Tuffnell, J. M.; Knebel, A.; Bennett, T. D.; Wondraczek, L. Low-Temperature Melting and Glass Formation of the Zeolitic Imidazolate Frameworks ZIF-62 and ZIF-76 through Ionic Liquid Incorporation. *Adv. Mater. Technol.* **2022**, *7*, No. 2200343.

(22) Gao, F.; Bai, R.; Ferlin, F.; Vaccaro, L.; Li, M.; Gu, Y. Replacement Strategies for Non-Green Dipolar Aprotic Solvents. *Green Chem.* **2020**, *22*, 6240−6257.

(23) Byrne, F. P.; Jin, S.; Paggiola, G.; Petchey, T. H. M.; Clark, J. H.; Farmer, T. J.; Hunt, A. J.; Mcelroy, C. R.; Sherwood, J. Tools and Techniques for Solvent Selection: Green Solvent Selection Guides. *Sustain Chem. Process* **2016**, *4*, 7.

(24) Stolar, T.; Užarević, K. Mechanochemistry: An Efficient and Versatile Toolbox for Synthesis, Transformation, and Functionalization of Porous Metal-Organic Frameworks. *CrystEngComm* **2020**, *22* (27), 4511−4525.

(25) Afshariazar, F.; Morsali, A. The Unique Opportunities of Mechanosynthesis in Green and Scalable Fabrication of Metal−Organic Frameworks. *J. Mater. Chem. A Mater.* **2022**, *10*, 15332.

(26) Yuet Yan Wong, C.; Wing-Tat Choi, A.; Lui, M. Y.; Fridrich, B.; Horváth, A. K.; Mika, L. T.; Horváth, I. T. Stability of Gamma-Valerolactone under Neutral, Acidic, and Basic Conditions. *Struct. Chem.* **2017**, *28*, 423−429, DOI: 10.1007/s11224-016-0887-6.

(27) Skrjanc, A.; Byrne, C.; Zabukovec Logar, N. Green Solvents as an Alternative to Dmf in Zif-90 Synthesis. *Molecules* **2021**, *26* (6), 1573.

(28) Deneff, J. I.; Butler, K. S.; Reyes, R. A.; Sava Gallis, D. F. Harnessing Particle Size-Control and DNA-Oligo Functionalization in ZIF-76 for Biological Applications. *Adv. Mater. Interfaces* **2023**, *10*, 2201532.

(29) Paseta, L.; Malankowska, M.; Téllez, C.; Coronas, J. Fast Synthesis of Zeolitic Imidazolate Framework ZIF-94 Using NaOH and Recycling Reagents. *Mater. Chem. Phys.* **2023**, *295*, 127039.

(30) Peralta, D.; Chaplais, G.; Simon-Masseron, A.; Barthelet, K.; Pirngruber, G. D. Synthesis and Adsorption Properties of ZIF-76 Isomorphs. *Microporous Mesoporous Mater.* **2012**, *153*, 1−7.

(31) Nugroho, A. P.; Masruroh; Sakti, S. P. The Design and Optimization Process of Ball Mill to Reduce Particle Size of Calcium Carbonate Materials. In *AIP Conference Proceedings*; American Institute of Physics Inc., 2020; Vol. *2296*. DOI: 10.1063/5.0030531.

(32) Tolomeu, H. V.; Fraga, C. A. M. Imidazole: Synthesis, Functionalization and Physicochemical Properties of a Privileged Structure in Medicinal Chemistry. *Molecules* **2023**, *28* (2), 838.

(33) Jerez, G.; Kaufman, G.; Prystai, M.; Schenkeveld, S.; Donkor, K. K. Determination of Thermodynamic PKa Values of Benzimidazole and Benzimidazole Derivatives by Capillary Electrophoresis. *J. Sep Sci.* **2009**, *32* (7), 1087−1095.

(34) Bumstead, A. M.; Thorne, M. F.; Sapnik, A.; Castillo Blas, C.; Lampronti, G. I.; Bennett, T. D. Investigating the Chemical Sensitivity of Melting in Zeolitic Imidazolate Frameworks. *Dalton Transactions* **2022**, *51*, 13636.

https://doi.org/10.1021/acs.cgd.3c00137
Cryst. Growth Des. 2023, 23, 3754−3760